Bioorganic Chemistry 179 (2026) 109997

Contents lists available at ScienceDirect

Bioorganic Chemistry

journal homepage: www.elsevier.com/locate/bioorg

Synthesis and biological evaluation of mixed aryl-alkyl succinates as modulators of autophagy and apoptosis in gastric carcinoma

Diego Olivieri [a], Michele Mari [a], Michela Battistelli [a,*], Sabrina Burattini [a], Carla Carfagna [b], Federico Gianfanti [a,*], Francesco Onesimo [a], Giovanni Bottegoni [a], Riham Osman [a], Nour Annous [a], Sara Salucci [c], Ilaria Versari [c], Irene Faenza [c], Matteo Micucci [a,1], Michele Retini [a,1]

[a] Department of Biomolecular Sciences, University of Urbino Carlo Bo, 61029 Urbino, Italy
[b] Department of Industrial Chemistry "Toso Montanari", University of Bologna, Via Piero Gobetti 85, 40129 Bologna, BO, Italy
[c] Department of Biomedical and NeuroMotor Sciences, University of Bologna, 40126 Bologna, Italy

ARTICLE INFO

Keywords:
Succinate derivatives
Gastric cancer
Carbonylation
Apoptosis
Hydroquinone esters

ABSTRACT

Vitamin E succinate and its derivatives have demonstrated encouraging cytotoxic potential in preclinical models of gastric cancer, paving the way for a novel class of therapeutics. Building on a previously described synthetic methodology based on the alkoxy-aryloxycarbonylation of alkenes, this study reports the investigation of the antitumor effects in gastric cancer models of mixed aryl-alkyl succinates esters featuring various substituents on the backbone. Nine compounds were screened for cytotoxicity against AGS and KATO III gastric cancer cell lines. The most active compounds – **2d** (R = $(CH_2)_4CH_3$), **2a** (R = Ph), and **2c** (R = CH_2CH_2Ph) – were further evaluated for efficacy, with **2d** emerging as the most potent agent (IC_{50} 30.9 μM in AGS; IC_{50} 19 μM in KATO III). Mechanistically, **2d** enhanced the expression of activated/cleaved Caspase-3, augmented PARP cleavage, and promoted LC3B lipidation – indicative of programmed cell death. Consistently, ultrastructural analysis of **2d**-treated cancer cells revealed morphological hallmarks of both early and late apoptosis, including cytoplasmic vacuolization and autophagic vacuoles. Conversely, treatment with compound **2d** did not affect the expression of apoptosis markers in healthy GES-1 gastric epithelial cells, suggesting a favorable safety profile. Overall, our findings provide insights into how specific structural features of succinate derivatives contribute to their anti-tumor activity, laying the groundwork for the design of more potent succinate-based agents.

1. Introduction

Gastric carcinoma, the third leading cause of cancer-related mortality globally, presents substantial challenges in oncology, primarily due to late-stage diagnosis and the constrained scope of the currently available therapeutic options. Despite significant strides in unravelling its pathophysiological underpinnings, the prognosis for patients with advanced-stage malignancy remains poor, with five-year survival rates of about 20% for cardia and 31% for non-cardia gastric cancer [1]. The etiopathogenesis of gastric cancer is multifactorial, involving both modifiable risk factors – such as lifestyle choices, tobacco use, alcohol consumption, and diet – and non-modifiable ones, including genetic predispositions, age, and *Helicobacter pylori* infection [2–6]. The therapeutic management of gastric cancer primarily relies on surgical resection, which represents the cornerstone of care for early-stage disease. This approach is often supplemented by adjuvant therapies, including chemotherapy and radiation therapy, aimed at eradicating microscopic residual lesions and reducing the risk of recurrence [7,8]. Commonly employed chemotherapeutic agents include cisplatin, a platinum-based compound, and doxorubicin, an anthracycline. These molecules are frequently used in combination regimens with other drugs such as fluorouracil (5-FU) and capecitabine to enhance therapeutic efficacy [9,10]. Unfortunately, the effectiveness of such treatments diminishes significantly in advanced stages of the disease, due to the emergence of aggressive phenotypes and resistance mechanisms that collectively hinder disease control [11,12]. The advent of targeted

* Corresponding authors.
E-mail addresses: michela.battistelli@uniurb.it (M. Battistelli), federico.gianfanti@uniurb.it (F. Gianfanti).
[1] These authors contributed equally to this work.

https://doi.org/10.1016/j.bioorg.2026.109997
Received 22 January 2026; Received in revised form 1 May 2026; Accepted 14 May 2026
Available online 16 May 2026

therapies has introduced a novel paradigm in gastric cancer treatment by targeting specific molecular alterations associated with disease progression. Trastuzumab, a monoclonal antibody against HER2, has demonstrated favorable outcomes in HER2-positive gastric cancer, providing a tailored approach that improves overall survival in this subset of patients [13,15]. Similarly, ramucirumab, a VEGFR-2 antagonist, has been approved as a second-line therapy for advanced or metastatic gastric adenocarcinoma, where it has demonstrated improvements in overall survival [16,17]. Despite these advances, the prognosis for advanced malignancies remains poor, with median survival in metastatic settings generally below one year. The limited clinical benefit and significant toxicity associated with existing treatment modalities underscore the pressing need for novel therapeutic approaches capable of broadening efficacy while minimizing adverse effects. Such therapeutics may arise from investigations into molecular-targeted agents, immunotherapies, and novel drug conjugates, aiming to provide more personalized and tolerable therapeutic options [18]. In this context, α-tocopheryl succinate derivatives are emerging for their anti-tumor properties against gastric carcinoma. These compounds modulate programmed cell death in a dose- and time-dependent manner. Notably, the synthetic derivative Val-Cit-PEG-Apoptogen (VCPA) has shown significant cytotoxic effects against gastric cancer cells by inducing ROS-driven apoptosis and mitochondrial dysfunction. Moreover, VCPA treatments enhanced the efficacy of doxorubicin, revealing a synergistic potential. Overall, these findings highlight the promise of targeting mitochondrial functions, signaling cascades, and ER stress pathways in gastric cancer, representing a multifaceted avenue for developing novel therapeutic strategies aimed at improving patient outcomes [19–24]. Building on this evidence, the development of alternative succinate derivatives containing different substituents both on the ester moiety and on the side chain of the succinate scaffold may further improve their effectiveness in combating gastric carcinoma. Based on previous expertise in oxidative carbonylation reactions [25–30], some of us recently reported an innovative methodology for the alkoxy-aryloxycarbonylation of alkenes, enabling the one-pot, regioselective synthesis of a novel class of succinic esters bearing both alkyl and aryl substituents on the ester functionalities [25]. Building on this approach, a series of succinate derivatives incorporating hydroquinone ester moieties was obtained [25]. In 2018, the anticancer activity of hydroquinone was evaluated both in vitro and in vivo across a range of cancer cell lines and tumor-bearing mouse models, demonstrating its therapeutic potential [31]. In addition, natural hydroquinone-derived compounds are known to display significant biological activities, including antioxidant properties [32], and recently, hydroquinone esters have been reported to exhibit in vitro cytotoxicity, particularly against A375 melanoma cells [33]. In light of these considerations, a series of mixed succinates containing both a hydroquinone ester and an alkyl ester, and displaying diverse substitution patterns on both the ester groups and the succinate backbone, along with selected analogues bearing different alkyl ester functionalities (Fig. 1), were screened for their antitumoral potential by evaluating their cytotoxicity against two gastric cancer cell models: human gastric adenocarcinoma AGS and poorly differentiated metastatic KATO III cells. Among them, the most cytotoxic compounds – **2a**, **2c**, and **2d** – were further evaluated for efficacy by calculating IC_{50} values in both AGS and KATO III cells. The most potent compound, 1-(4-hydroxyphenyl) 4-isopropyl 2-pentylsuccinate **2d**, was then investigated for its morphological effects on cancer cells and its ability to modulate key biological processes involved in gastric cancer pathogenesis, including both type I and type II programmed cell death. Through these investigations, we aim to elucidate the mechanisms by which these previously untested succinate derivatives exert their anticancer effects, focusing on the modulation of programmed cell death pathways. Our findings represent a pivotal step toward the development of succinate-based therapeutics, offering new perspectives for improving treatment modalities and clinical outcomes in gastric carcinoma.

2. Materials and methods

2.1. Chemistry

The succinate derivatives have been synthesized according to known literature procedures [25,29,30,34]. ^{1}H NMR spectra of known compounds **2a-2f** [25], **2 g** [30], and **2i** [34] are in accordance with literature data, and copies of the spectra are given in the Supporting Information. Characterization data and copies of ^{1}H and ^{13}C NMR spectra for the new compound **2 h** are reported in the Supporting Information. All compounds were isolated as racemic mixtures. ^{1}H NMR and ^{13}C NMR were recorded on a Bruker Avance 400 spectrometer (^{1}H: 400 MHz, ^{13}C: 101 MHz), using $CDCl_3$ as solvent. Chemical shifts are reported in the δ scale relative to residual $CHCl_3$ (7.26 ppm) for ^{1}H NMR and to the central line of $CDCl_3$ (77.16 ppm) for ^{13}C NMR. ^{13}C NMR were recorded with ^{1}H broadband decoupling. Coupling constants (*J*) are reported in Hertz (Hz). The purity of the compounds was judged by ^{1}H NMR spectroscopy [35] and high-pressure liquid chromatography for compounds bearing a chromophoric group (**2a-2f**). All the tested compounds had purity greater than 95% except for derivative **2e**. HPLC analyses were performed on Agilent 1260 Infinity II HPLC/UV system using Agilent Polaris C18 5 mm, 250 × 4.6 mm column. The mobile phase consisted of acetonitrile and water (containing 0.1% formic acid). A linear gradient of 60% to 100% acetonitrile over 10 min was used except for **2e**, which required a linear gradient of 80% to 100% over the same duration. Flow rate of 1 mL/min. λ = 254 or 270 nm. Injection volume 20 mL. For solid samples, melting points (mp) were determined on capillary melting point apparatus and are uncorrected. ESI-MS spectra were recorded on Waters Micromass ZQ 4000, using electrospray ionization techniques, with samples dissolved in MeOH or CH_3CN. HRMS spectra were performed by slow direct infusion (5 μL/min) of ≈ 0.1 μg/mL solution (methanol), using Orbitrap Exploris 240 mass spectrometer. Only molecular ions $[M + H]^+$ are given. For compound **2 g** the molecular ion was detected as $[M + Na]^+$. Before charging carbon monoxide, all reactions were prepared under a nitrogen atmosphere using dry solvents under anhydrous conditions, in a stainless-steel autoclave, by using the Schlenk technique. Carbon monoxide (Cp

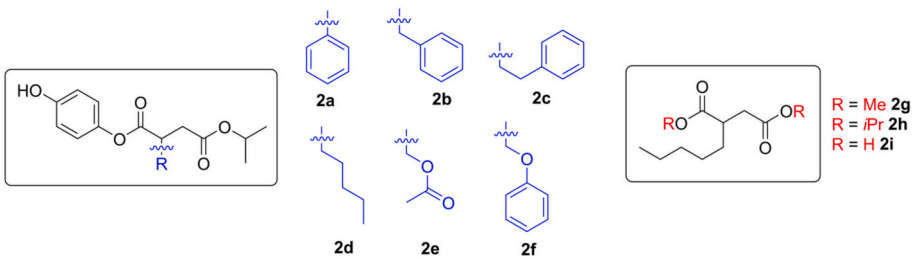

Fig. 1. Succinate derivatives synthesized via alkoxy-aryloxycarbonylation or bis-alkoxy carbonylation of alkenes and evaluated for cytotoxic activity against gastric cancer cells.

grade 99.99%) was supplied by Air Liquide. Caution: Carbon monoxide is a toxic gas with potentially lethal action; therefore, adequate precautions must be observed. The *p*-benzoquinone was purchased by Merck Sigma-Aldrich and was filtered off a plug of silica gel, washing with CH_2Cl_2, obtaining a yellow solid after drying the solution under vacuum. Pure compounds **2** were isolated through flash column chromatography on silica gel 60 (40–60 μm, 230–400 mesh). Olefins **1** were purchased from Merck Sigma-Aldrich, filtered off a plug of neutral Al_2O_3, and used without further purification. Anhydrous THF was distilled from sodium-benzophenone, and methanol was distilled from $Mg(OMe)_2$. Isopropanol was dried over molecular sieves (Alfa Aesar, 4 Å, 1–2 mm, beads). Hydroquinone was utilized as purchased by Merck Sigma-Aldrich. Pd $(TFA)_2$ was purchased by Fluorochem. All other chemicals were purchased from Merck Sigma-Aldrich and used without further purification. Ligands **L1** [36] and **L2** [37] were synthesized according to the literature. All solid reagents were weighed in an analytical balance without excluding moisture and air. Property predictions were performed using QikProp as implemented in Schrödinger 2025–02 (Schrödinger, New York, NY, USA). Structural alerts were assessed using the assignSubstructureFilters.py Python script described by Schuffenhauer and co-workers [38].

2.2. Cell culture and reagents

AGS and KATO III human gastric cancer cell lines were obtained from ATCC (American Type Culture Collection, Manassas, VA, USA). AGS cells, derived from a gastric adenocarcinoma in a female patient, were cultured in DMEM/F12 medium (Gibco, Thermo Fisher Scientific, Waltham, MA, USA) enriched with 100 U/mL penicillin, 100 mg/mL streptomycin, 2 mM L- glutamine (Gibco, Thermo Fisher Scientific, Waltham, MA, USA), and 10% heat-inactivated fetal bovine serum (FBS, Euroclone Milano, Italy). KATO III cells, isolated from the tumor tissue of a 55-year-old Asian male, were grown with Iscove's Modified Dulbecco's Medium (IMDM; 30–2005™, ATCC) supplemented with 20% FBS. GES-1 cells, a noncancerous gastric epithelial immortalized cell line derived from normal gastric epithelial tissue, were cultured in RPMI-1640 medium (Gibco, Thermo Fisher Scientific, Waltham, MA, USA) supplemented with 10% FBS, penicillin 100 U/mL, streptomycin 100 mg/mL, and 1% L-glutamine (Gibco, Thermo Fisher Scientific, Waltham, MA, USA). All cell lines were kept at 37 °C in a humidified atmosphere containing 5% CO_2 [39]. Each newly synthesized succinate derivative was dissolved in DMSO to prepare stock solutions of 2 mM, which were subsequently diluted in growth medium before being added to the cells.

2.3. MTT assay

The cytotoxic potential of the synthesized compounds on gastric cancer cells was assessed employing the MTT assay. Ten thousand AGS, KATO III, or GES-1 cells were seeded into 96-well plates and maintained in a humidified incubator for 24 h. Afterwards, the medium was replaced with 100 μL of fresh medium containing each single compound at concentrations ranging from 0 to 500 μM. Cancer cells exposed to an equivalent concentration of DMSO were considered the control group. Moreover, cancer cells have been treated with cisplatin (CPPD). The plates were incubated for an additional 72 h. Afterwards, each well was supplemented with 10 μL of MTT solution (R&D Systems, Minneapolis, MN, USA) and incubated for 3 h at 37 °C. Lastly, the purple formazan crystals, generated by the metabolically active cells, were dissolved with 100 μL of Detergent Reagent (R&D Systems, Minneapolis, MN, USA). The resulting absorbance was measured at 570 nm using a microplate reader. Based on absorbance values, the cytotoxicity of the succinate derivatives on cells was evaluated [40]. GraphPad Prism v.9.0 (GraphPad Software, La Jolla, CA, USA) was employed to generate the dose-response graphs. IC_{50} values for each compound were calculated using a nonlinear regression model, namely log(inhibitor) vs. normalized response, standard slope (Hill slope = −1), confidence intervals (CI) 95%.

2.4. Protein extraction and Western blotting (WB)

Protein extraction was carried out using radioimmunoprecipitation assay (RIPA) lysis buffer supplemented with EDTA-free protease and phosphatase inhibitor cocktails (Thermo Fisher Scientific). Lysates were vortexed for 30 min at 4 °C and centrifuged at 4000 ×*g* for 15 min at 4 °C to remove cellular debris. Protein concentrations were then determined using the Pierce BCA Protein Assay Kit (Thermo Fisher Scientific). Afterwards, proteins were separated by sodium dodecyl sulfate-polyacrylamide gel electrophoresis (SDS-PAGE) on 4–12% gradient gels and subsequently transferred to membranes for immunoblotting. Membranes were incubated with the following primary antibodies: anti-cleaved Caspase-3 (Cat. No. 9661, 1:1000), anti-Beclin-1 (Cat. No. 3738S, 1:1000), anti-PARP (Cat. No. 9542, 1:1000) and anti-LC3B (Cat. No. 2775S, 1:1000) from Cell Signaling Technology (Beverly, MA, USA); anti-tubulinβ (Cat. No. sc-166,729, 1:1000) and anti-Bcl-x S/L (Cat. No. sc-1041, 1:1000) from Santa Cruz Biotechnology (Dallas, TX, USA). Following primary antibody incubation, membranes were washed four times with PBS containing 0.1% Tween-20 and then incubated for 1 h at room temperature (RT) with a horseradish peroxidase (HRP)-conjugated secondary antibody diluted 1:10,000 in PBS-Tween-20. After four additional washes, protein bands were visualized using the iBright Imaging System (Invitrogen) following incubation with Westar Antares ECL substrate (Cyanagen, Bologna, Italy) [41].

2.5. Transmission electron microscopy (TEM)

Cells were first fixed for 1 h at RT with 2.5% glutaraldehyde in 0.1 M phosphate buffer. Following fixation, samples were washed, post-fixed for 1 h at RT in 1% osmium tetroxide (OsO_4) and dehydrated through a graded ethanol series. Subsequently, the samples were embedded in epoxy resin at 60 °C for three days. Semi-thin sections were treated with toluidine blue and observed under a light microscope. Ultrathin sections were contrasted with UranyLess and lead citrate, then examined using a Philips CM10 Electron Microscope. Cell viability has been evaluated by means of a light microscope (100 mm^2 of area) able to distinguish healthy cells, early and late apoptotic cells, and necrotic ones. These features have been inserted in Fig. 9 as representative micrographs. Morphometric analyses were performed to quantify the number of total autophagic vacuoles and that of autophagosomes and autophagolysosomes in control and treated conditions, both in AGS and KATO cells. In detail, the subcellular organelles have been counted considering for each condition an area of 12 mm^2. The same area was used to evaluate the mitochondrial size and the number of cristae in control and treated samples. Furthermore, in AGS- and KATO-treated cells, we quantified the number of damaged mitochondria surrounded by phagophore, indicative of mitophagy activation [42].

2.6. Scanning electron microscopy (SEM)

AGS and KATO III cells, grown under adherent and semi-adherent conditions, respectively, were washed and subsequently fixed for 1 h with 2.5% glutaraldehyde in 0.1 M phosphate buffer. Following fixation, the samples were treated with 1% OsO4 for 1 h and then dehydrated through a graded ethanol series. Lastly, the specimens were critical-point dried, gold-sputtered, and examined using a Philips 515 scanning electron microscope [42].

2.7. Statistical analysis

The reliability and accuracy of the results were evaluated through rigorous statistical analysis. First, the Shapiro-Wilk test was performed to assess data normality. As the dataset followed a normal distribution,

statistical comparisons were conducted using either one-way or two-way analysis of variance (ANOVA), or a *t*-test, as appropriate. Post-hoc analyses were performed using either Šídák's or Dunnett's multiple comparisons test to compare each treated group with the control group. All statistical analyses were carried out using GraphPad Prism software. MTT assay results are reported as mean ± SD from three independent experiments (**Table S1**). Morphometric data are presented as specified in the corresponding figure legends. Statistical significance was expressed as $P < 0.05$ (*), $P < 0.01$ (**), $P < 0.001$ (***), and $P < 0.0001$ (****).

3. Results

3.1. Chemical synthesis of succinate derivatives

The succinate derivatives **2a-f** were synthesized using a reported one-pot regioselective procedure [25] that involves the alkoxy-aryloxycarbonylation of alkenes in the presence of an aliphatic alcohol and a phenol derivative at room temperature and 4 bar of CO (Fig. 1). The reaction proceeds using an aryl α-diimine palladium (II) catalyst, formed in situ by mixing Pd(TFA)2 and ligand **L1**, and *p*-benzoquinone is eventually necessary to oxidize the Pd(0) species that is eventually generated after the carbonylative coupling of the involved nucleophiles (i.e., alkenes, alcohols, and phenols). A series of 1-(4-hydroxyphenyl) 4-isopropyl succinates, differing at the succinate skeleton, was synthesized as reported in Scheme 1A, using hydroquinone and isopropanol. To understand the role of the ester moiety on the biological activity observed for compound **2d**, three analogues bearing a pentyl chain in position 2 of the succinate have been synthesized. Other than the already known dimethylsuccinate compound **2 g** [30], the diisopropylsuccinate **2 h** has also been synthesized (Scheme 1B) following a reported bis-alkoxycarbonylation reaction [29], while the 2-pentylsuccinic acid **2i** is obtained by the hydrolysis of **2 g** (Scheme 1C) [34].

3.2. Cytotoxicity against gastric cancer cells

The antitumor potential of the synthesized compounds **2a-f** was assessed using the MTT assay, following the experimental design illustrated in Fig. 2. Human gastric adenocarcinoma AGS cells and human signet ring cell carcinoma KATO III cells were treated with increasing concentrations of each compound for 72 h, and cell viability was evaluated to identify the most cytotoxic candidates (Fig. 3). Among the tested compounds, **2a**, **2c**, **2d** and **2e** exhibited cytotoxic activity against gastric cancer cells. However, **2e** failed to reduce AGS cell viability and was thus excluded for not fulfilling the efficacy requirements (Filter 1). The selected candidates were subsequently compared by calculating their IC_{50} values using non-linear regression analysis (Filter 2). Succinate **2d** – bearing a linear aliphatic chain as a substituent on the succinate backbone – exhibited the highest cytotoxic potential against both AGS and KATO III cells, with IC_{50} values of 30.9 μM and 19 μM, respectively. The calculated R^2 value of 0.81 for both cell lines indicates a strong goodness-of-fit, underscoring a robust dose-dependent effect (Fig. 4A). Compound **2d** was also evaluated in normal epithelial GES-1 cells, showing a calculated IC_{50} value of 38.3 μM (Fig. 4A). Compound **2a** – featuring a phenyl group on the succinate backbone – was less effective in reducing gastric cancer cell viability. KATO III cells were more sensitive to **2a** than AGS cells, as evidenced by a lower IC_{50} value (76.9 μM vs. 117.8 μM) and a higher R^2 coefficient (0.81 vs. 0.74), reflecting a more consistent dose-response relationship (Fig. 4B). Lastly, **2c** – bearing a homobenzylic moiety – exhibited slightly greater cytotoxicity in KATO III cells (IC_{50} 54.4 μM, R^2 0.75) compared to AGS cells (IC_{50} 56.3 μM, R^2 0.58) (Fig. 4C). As shown in Fig. 4D, KATO III and AGS cells have also been treated with CPPD and the IC_{50} values are 16.9 and 17 μM, respectively. Overall, **2d** emerged as the most potent succinate derivative, followed by **2c**, while **2a** showed the weakest antiproliferative activity. These findings seem to suggest that less rigid substituents – such as hydrocarbon chains – enhance cytotoxic activity, likely due to more efficient cellular uptake and interaction with intracellular molecular targets. Moreover, compared to fully aliphatic chains, the presence of aromatic groups leads to reduced potency, possibly due to increased molecular rigidity or steric reasons. Notably, three structural analogues of **2d** – namely **2 g**, **2 h**, and **2i** – in which the hydroquinone moiety on the ester was replaced with alternative groups (i.e., OMe, O*i*Pr, OH), failed to display any antitumor activity. This indicates that, beyond modifications to the succinate backbone, the hydroquinone moiety plays a pivotal role in orchestrating the observed cytotoxic effects. The results discussed above are summarized in Fig. 5, motivating the choice of **2d** for further studies aimed at elucidating the molecular mechanisms underlying its anti-tumoral activity.

3.3. Compound 2d modulates autophagy and triggers caspase-dependent apoptosis

To investigate the molecular events associated with the cytotoxic

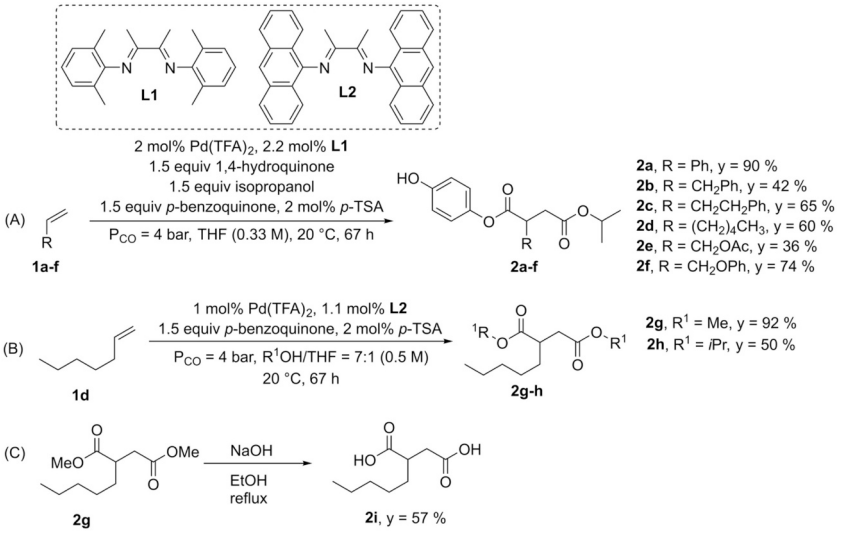

Scheme 1. Regioselective alkoxy-aryloxycarbonylation of alkenes for the synthesis of compounds **2a-f.** For compounds **2b**, **2e** and **2f**, 5 mol% of catalyst loading was utilized with olefin concentration = 0.5 M (**A**). Bis-alkoxy carbonylation of alkenes for the synthesis of compounds **2 g-h**. For compound **2 h**, 2 mol% of catalyst loading was utilized in the presence of ligand **L1** (**B**). Hydrolysis of **2 g** for the synthesis of 2-pentylsuccinic acid **2i** (**C**).

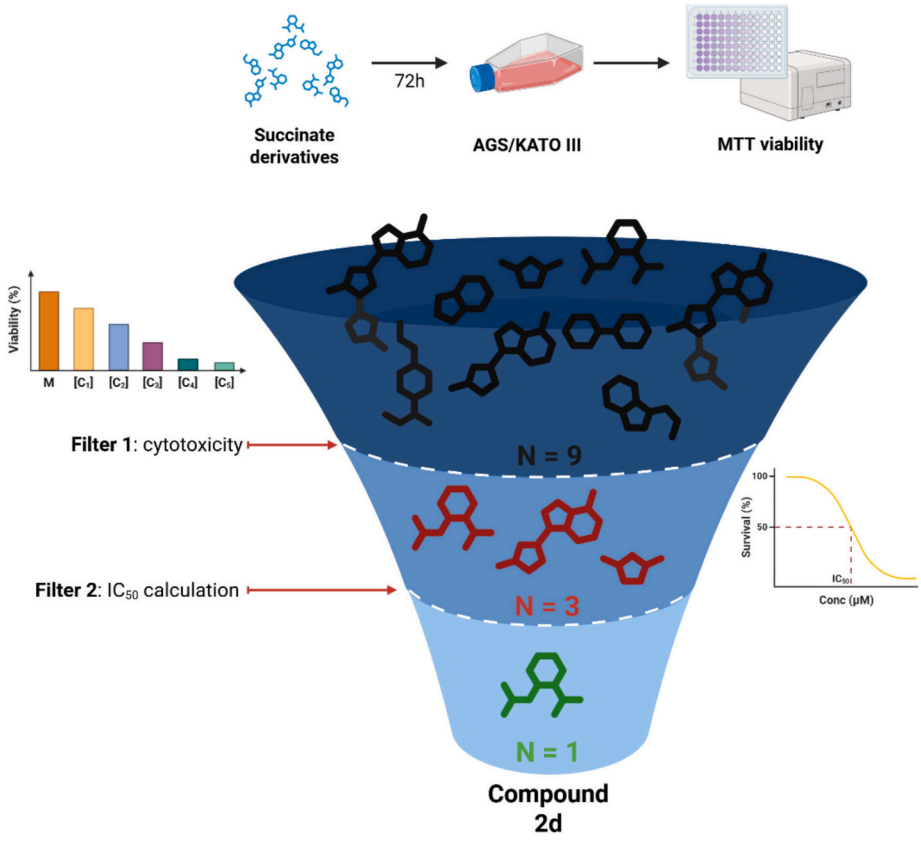

Fig. 2. Representation of the screening experimental design, illustrating the sequential filters applied and the number of compounds evaluated at each stage. **Filter 1** (cytotoxicity filter) assessed the cytotoxic potential of the compounds against both AGS and KATO III cell lines. **Filter 2** provided a comparison of IC_{50} values. A total of nine compounds ($N = 9$) were initially tested. Three candidates ($N = 3$) passed the cytotoxicity filter and were subsequently tested for potency based on their IC_{50} values. Cell viability was assessed using the MTT assay.

activity of **2d**, the expression of protein effectors involved in the regulation of type I (apoptosis) and type II (autophagy) programmed cell death was examined by WB in cells treated with 30 μM **2d** for 24 h (Fig. 6). Interestingly, the modulation of these pathways appeared to be cell-type dependent, as evidenced by distinct expression patterns observed in AGS and KATO III cells. In AGS cells, treatment with **2d** strongly induced the expression of activated/cleaved Caspase-3, along with a significant increase in PARP cleavage, as indicated by the appearance of the 89 kDa fragment. This pattern is consistent with proteolytic activation and the initiation of apoptosis. Of note, **2d** treatment also caused a mild reduction in the expression of the autophagy initiator Beclin-1. Concomitantly, AGS-treated cells displayed clear activation of the autophagosome marker LC3B, as highlighted by the appearance of its lipidated form, LC3B-II. In contrast, the expression of the anti-apoptotic marker Bcl-xL was not affected by the treatment, maintaining basal expression levels. In KATO III cells, apoptosis-related proteins were modulated in a similar fashion. Cleaved PARP fragments accumulated following treatment, along with a less pronounced activation of Caspase-3. Interestingly, Beclin-1 expression was only slightly downregulated, whereas LC3B lipidation – and consequent activation – was clearly enhanced in response to **2d**. Unlike AGS cells, Bcl-xL expression in KATO III cells was slightly upregulated by the treatment. Overall, these molecular profiles support a programmed cell death-oriented phenotype, as evidenced by PARP cleavage, a downstream marker of apoptosis. This effect is particularly evident in AGS cells, while KATO III cells display a more complex, autophagy-oriented molecular response. In addition, the same markers have been evaluated in healthy epithelial GES-1 cells exposed to **2d** compound. Notably, compound **2d** did not alter apoptotic and autophagic targets in this non-tumorigenic cell model (Fig. 6).

3.4. Compound 2d induces mitochondrial damage, autophagic vacuole formation and accumulation of apoptotic bodies in gastric cancer cells

To examine the morphological effects of **2d**, SEM and TEM ultrastructural analyses were conducted on AGS and KATO III cells under baseline conditions and following a 24-h treatment with 30 μM **2d**. In line with the biochemical findings described in the previous section, exposure to **2d** induced morphological changes consistent with cell death (Figs. 7, 8). As illustrated in Fig. 7, AGS control cells appeared polygonal (Fig. 7A) and elongated (Fig. 7B), with preserved nuclear architecture (Fig. 7B), intact cytoplasmic organelles (Fig. 7C, D), in particular well-preserved mitochondria (Fig. 7D), and seamless plasma membranes. In contrast, treated AGS cells displayed typical apoptotic features: membrane blebbing (Fig. 7E), chromatin condensation together with the detachment of nuclear membrane (Fig. 7F), micronuclei presence, and the accumulation of apoptotic bodies (Fig. 7G). Furthermore, a high number of autophagic vacuoles appeared in the cytoplasm (Fig. 7H). KATO III cells under control conditions preserved their ultrastructural integrity (Fig. 8): the cells showed high confluence (Fig. 8A) and intact nuclear structure and subcellular organelles (Fig. 8B). In contrast, treated cells exhibited a reduced confluence with apoptotic and necrotic patterns (Fig. 8C). A high number of cells showed diffuse vacuolization and the loss of plasma membrane integrity (Fig. 8D), as well as empty or swollen mitochondria (Fig. 8E). Because ultrastructural analysis indicated a high proportion of dead cells after exposure to compound **2d**, cell viability was further evaluated by direct cell counting using light microscopy. We evaluated the number of viable, apoptotic (early and late events) and necrotic cells under baseline conditions and following treatment with **2d** (Fig. 9). Viable cells were identified by their preserved morphology (Fig. 9A). Early apoptotic

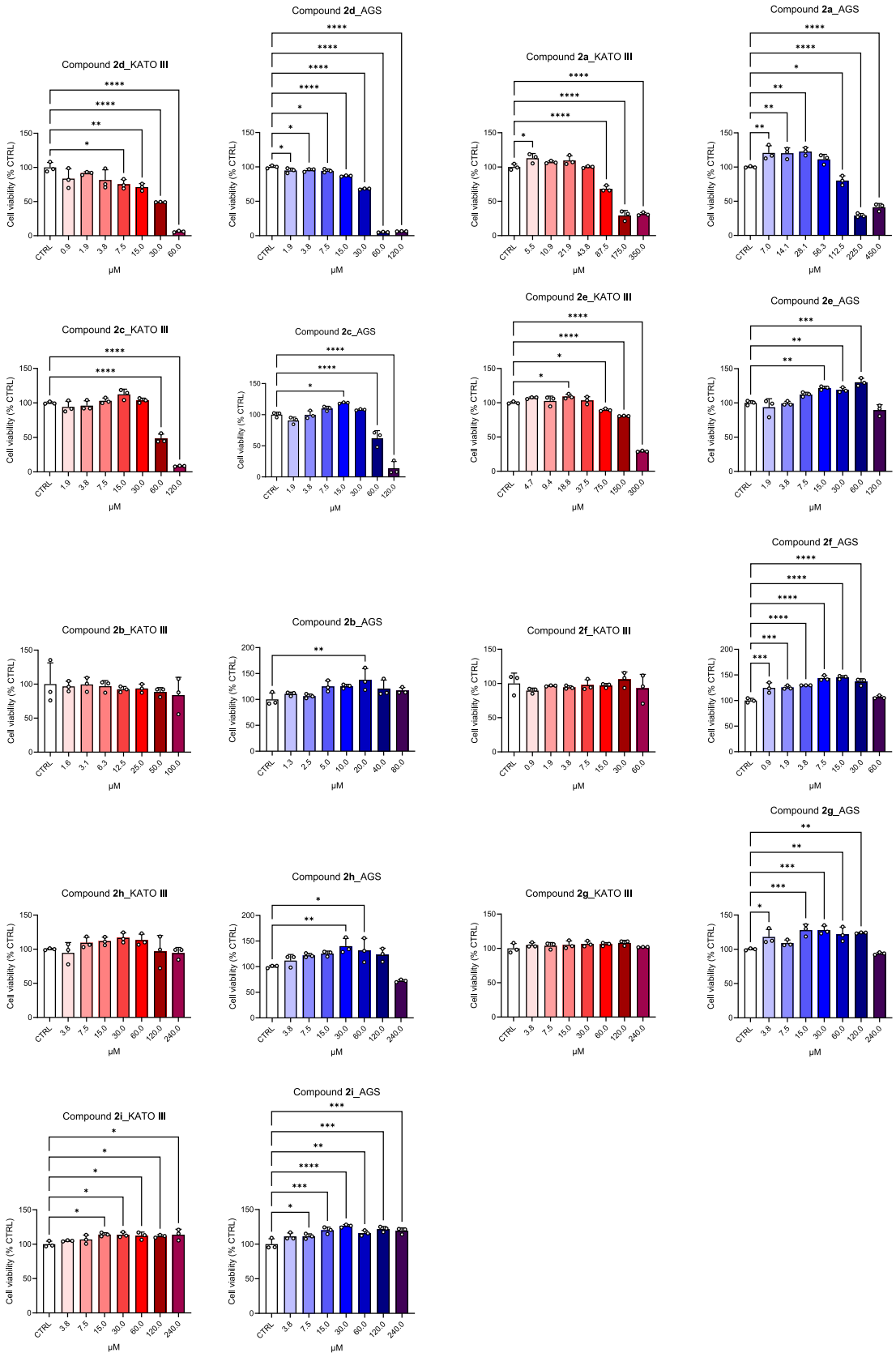

Fig. 3. Evaluation of the cytotoxic activity of nine synthesized succinate derivatives in gastric cancer cells. AGS and KATO III cells were treated with increasing concentrations of each succinate derivative for 72 h, and cell viability was measured using the MTT assay. Data are presented as mean ± SD from three independent experiments. Statistical significance was determined by one-way ANOVA followed by Dunnett's multiple comparisons test, comparing treated cells to untreated controls (CTRL). $P < 0.05$ (*), $P < 0.01$ (**), $P < 0.001$ (***), and $P < 0.0001$ (****).

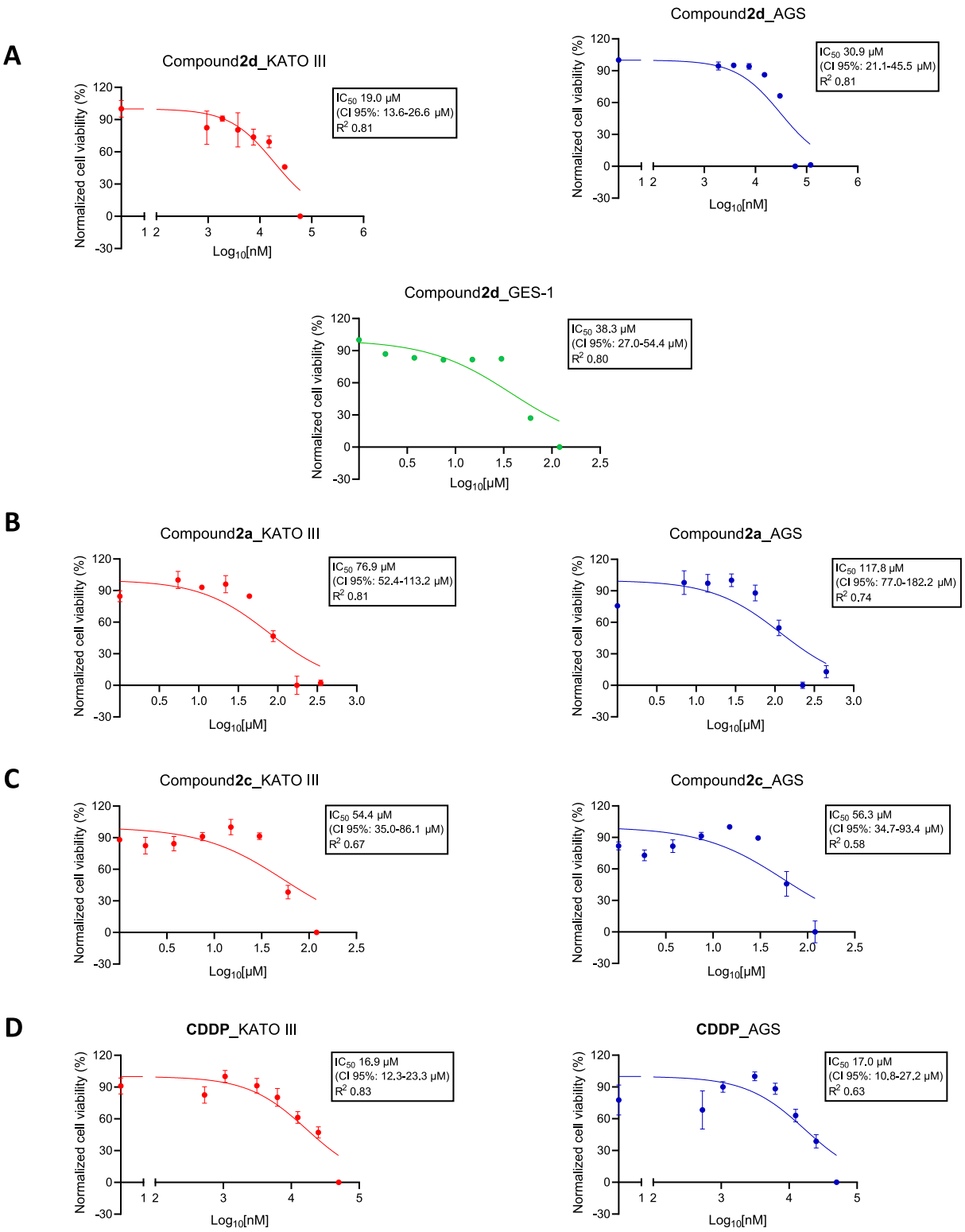

Fig. 4. Potency determination of **2d** (**A**), **2a** (**B**), and **2c** (**C**) and **CDDP** (**D**) in healthy and gastric cancer cells. AGS, KATO III, and GES-1 cells were treated with increasing concentrations of the three succinate derivatives and CDDP for 72 h, and cell viability was assessed using the MTT assay. Data are presented as mean ± SD from three independent experiments. IC_{50} values for each compound were calculated using a nonlinear regression model: log (inhibitor) vs normalized response, standard slope (Hill slope = −1), confidence intervals (CI) 95%.

cells were characterized by chromatin condensation (Fig. 9B), whereas late apoptotic cells exhibited the presence of micronuclei (Fig. 9C) and apoptotic bodies (Fig. 9D). Necrotic cells were defined by plasma membrane disruption and marked cytoplasmic vacuolization (Fig. 9E). Quantitative analysis confirmed a predominant increase in apoptotic cells for AGS exposed to **2d**, with a slight rise in necrotic events. On the contrary, **2d**-treated KATO III cells showed a prevalence of necrotic cell death (Fig. 9). Subsequently, given the activation of autophagic markers observed by WB and the presence of autophagic vacuoles at ultrastructural level in both gastric cancer cells exposed to **2d**, we focused on the

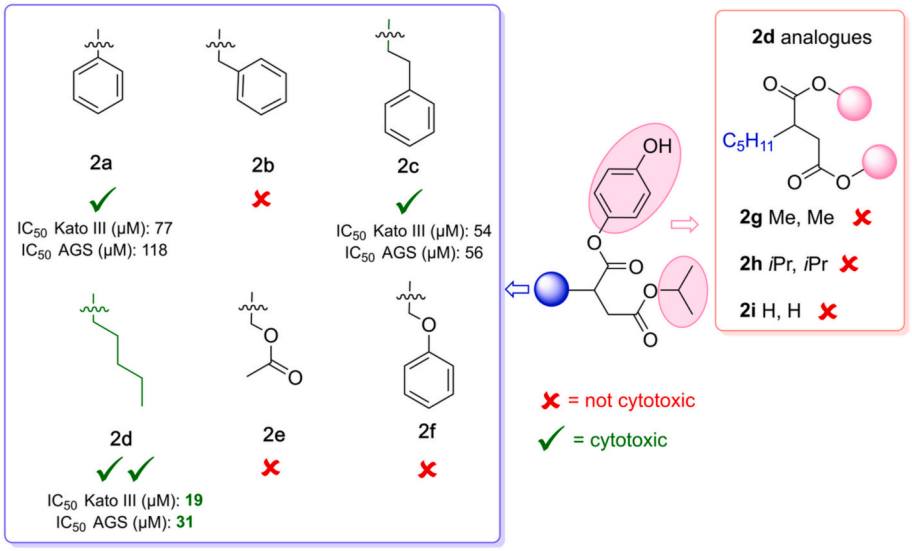

Fig. 5. SAR of compounds 2. IC_{50} values were determined only for cytotoxic compounds in KATO III and AGS cells. Compounds exhibiting cytotoxic effects at ≥120 μM were classified as "cytotoxic".

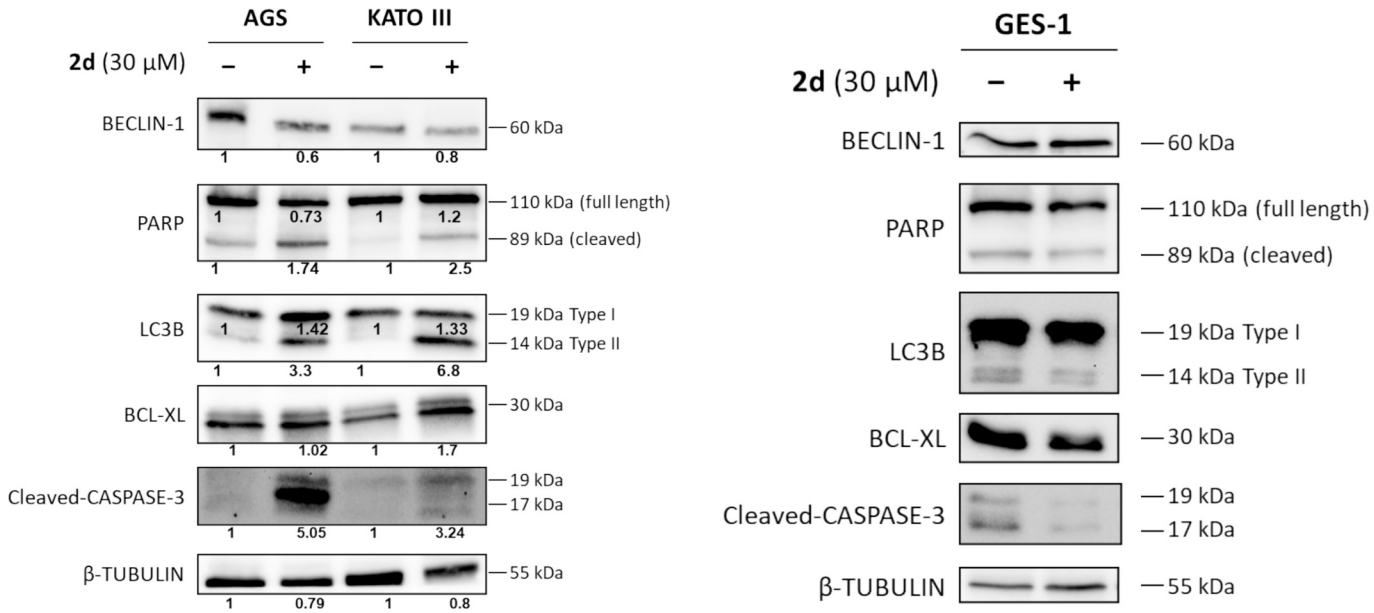

Fig. 6. WB analysis of programmed cell death-related proteins in AGS, KATO III, and GES-1 cells treated with **2d**. Representative pictures illustrating the expression of PARP, Caspase-3, and Bcl-xL (apoptosis- related), along with LC3B and Beclin-1 (autophagy-related) in AGS, KATO III, and GES-1 cells treated with 30 μM **2d** for 24 h, compared to vehicle-treated controls (CTRL). The images represent one of three independent experiments. Western blot bands were quantified by densitometric analysis.

evaluation of these structures through TEM morphometric analysis (Fig. 10), a widely recognized technique for the study of autophagy. We evaluated, under control conditions and following treatment with **2d** in both cancer cell lines, the number of autophagic vacuoles per cell and the presence of autophagosomes (Fig. 10A) and autophagolysosomes (Fig. 10B) per field. In both **2d**-treated cell lines, compared to the control ones, a significant number of autophagic vacuoles could be detected. In **2d**-treated AGS cells, autophagic structures are characterized by a high number of autophagosomes, reflecting an activation of the autophagic process aimed at the degradation of damaged organelles and protein aggregates. In contrast, treated KATO III cells showed a higher number of autolysosomes, indicating a more advanced stage of autophagy. However, this occurs in the context of widespread cellular damage, as previously described, characterized by disruption of the plasma membrane integrity. This may suggest that, despite the activation of autophagic flux, the extent of cellular injury is more severe and potentially irreversible. Furthermore, the behavior of mitochondria has been considered to understand their potential involvement in cell death induction. Consistently, morphometric analysis demonstrated that, on average, mitochondria in treated cancer cells were approximately twice the size of those under baseline conditions (0.95 vs 0.52 μm in AGS; 0.96 vs 0.55 μm in KATO III) (Fig. 11). In addition, the number of cristae significantly decreased in AGS and KATO III cells exposed to **2d** compared to untreated control conditions (9.4 vs 1.5 in AGS; 11.0 vs 1.4 in KATO III). To understand if damaged mitochondria are involved in mitophagy activation, we have quantified the number of damaged mitochondria surrounded by a phagophore (an initial double membrane that starts wrapping around cell material destined for degradation) in

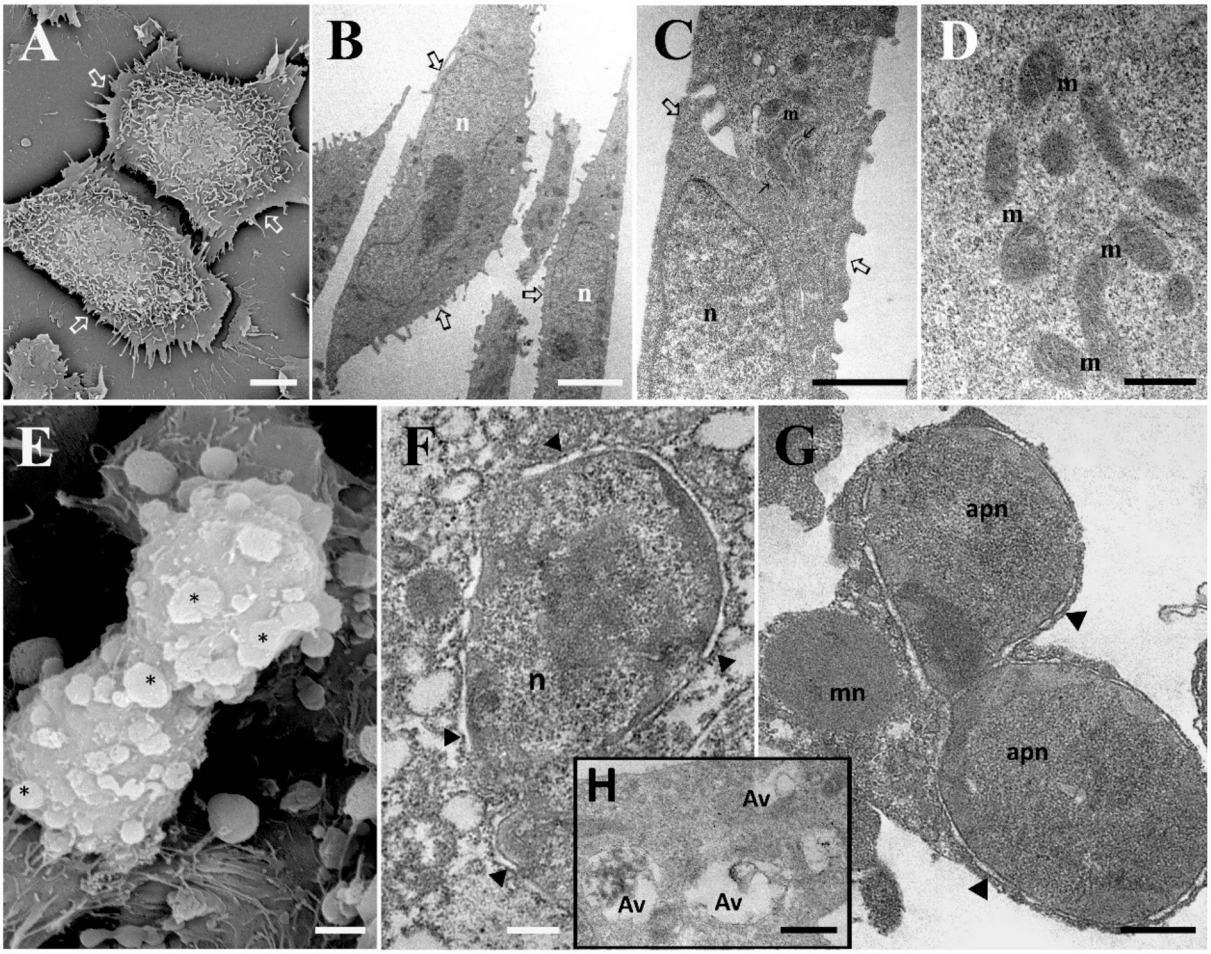

Fig. 7. Morphological characterization of AGS cells treated with compound **2d** for 24 h vs untreated cells. Untreated AGS, SEM (**A**) and TEM (**B**, **C**, **D**); treated AGS, SEM (**E**) and TEM (**F**—**H**). Control cells displayed polygonal (**A**) or elongated (**B**) morphology, with well-preserved nuclear architecture (**B**), intact cytoplasmic organelles (**C**, **D**) – including well-preserved mitochondria (**D**) – and intact plasma membranes. AGS-treated cells exhibited hallmark features of apoptosis, including membrane blebbing (**E**), chromatin condensation accompanied by nuclear membrane detachment (**F**), the presence of micronuclei, and the accumulation of apoptotic bodies (**G**). In addition, numerous autophagic vacuoles were observed within the cytoplasm (**H**), suggesting concurrent activation of autophagy. ⇒, plasma, plasma membrane; **n**, nucleus; **m**, mitochondria; *, membrane blebs; ▶, membrane detached; **Av**, autophagic vacuoles; **apn**, apoptotic nucleus, **mn**, micronuclei. Scale bars: **A**, 2 μm; **B**, **E** 500 nm; **C**, **G**, 250 nm; **D**, **F**, **H**, 100 nm.

2d-treated cancer cells. Mitochondria enclosed by phagophore membranes were more frequently observed in treated AGS cells compared to KATO III cells. This finding was consistent with the ultrastructural observations, which revealed, in treated AGS cells but not in control cells (Fig. 11A), damaged mitochondria exhibiting reduced cristae density and frequently surrounded by phagophore membranes (Fig. 11B). In KATO III control cells, mitochondria appeared structurally intact (Fig. 11C), whereas after **2d** treatment (Fig. 11D) they appeared disrupted and were, most of the time, not enclosed by phagophores, suggesting their involvement in the activation of cell death pathway.

3.5. *Computational analysis of the physicochemical properties*

From a physicochemical standpoint, the series occupies a tractable property space, with calculated $\log P_{o/w}$ values ranging from 1.8 to 4.4 and molecular weights spanning 188.2 to 358.4 Da. Compound **2d**, which showed the most favorable overall profile, has a calculated $\log P_{o/w}$ of 3.8 and a molecular weight of 322 Da, placing it well within a range considered amenable to further optimization. In addition, application of the comprehensive set of structural alerts compiled by Schuffenhauer et al. [38] for the assembly of the 2020 Novartis Small Molecule Screening Deck adopted to avoid problematic compounds, indicated a generally clean profile for the series. Only one compound, **2e**, triggered a low-severity alert, attributable to the presence of three ester functionalities, whereas no other compound received structural-alert flags. Compounds **2a-f** were annotated for the presence of a phenolic ester moiety, which is recognized primarily as a potential liability for long-term stock stability. Taken together, these results position the series as a promising starting point for further optimization, with proper toxicological profiling to be integrated as the compounds advance.

4. Discussion

Gastric cancer represents a significant global health challenge, ranking as the fifth most commonly diagnosed cancer and the third leading cause of cancer-related death worldwide. Its etiology is complex and multifactorial, involving genetic predispositions, environmental factors, and *Helicobacter pylori* infection [43]. Despite major advances in the molecular understanding of this disease, gastric cancer is often diagnosed at late stages, with five-year survival rates ranging from 20 to 31% [44]. This discouraging clinical outlook underscores the pressing need for alternative therapeutic strategies with enhanced efficacy against advanced gastric cancer phenotypes. Current therapeutic interventions include surgical resection for localized diseases, usually complemented by chemotherapy or radiation. In advanced malignancies, systemic therapies – such as cisplatin, 5-FU, and doxorubicin –

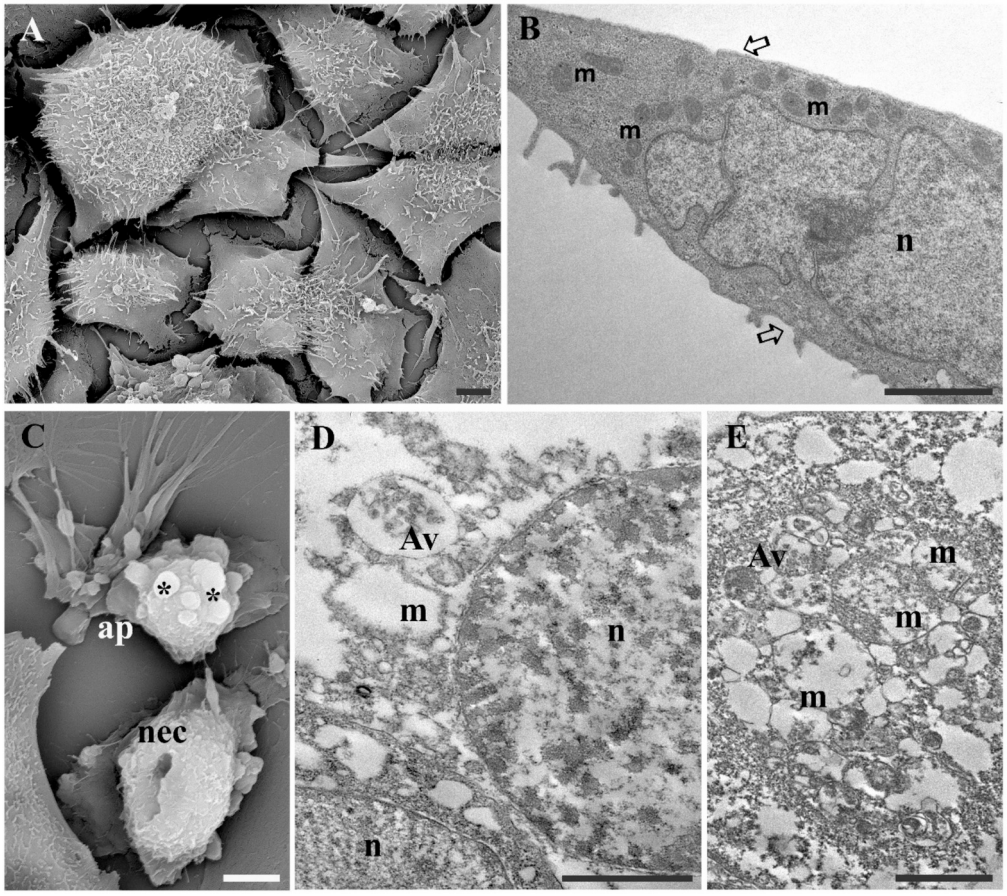

Fig. 8. Morphological characterization of KATO III cells treated with compound **2d** for 24 h vs untreated cells. Untreated KATO III, SEM (**A**) and TEM (**B**); treated KATO III, at SEM (**C**) and TEM (**D**, **E**). The cells exhibited high confluence (**A**), with intact nuclear architecture and well-preserved subcellular organelles, including mitochondria (**B**). In contrast, treated cells showed reduced confluence and features consistent with apoptotic and necrotic processes. In **C**, a cell exhibiting membrane blebbing, indicative of apoptosis, coexists with a neighboring cell that has lost plasma membrane integrity. Many cells displayed diffuse cytoplasmic vacuolization, compromised plasma membrane integrity (**D**), and swollen or empty mitochondria (**E**). ⇒, plasma membrane; **n**, nucleus; **m**, mitochondria; *, membrane blebs; **ap**, apoptotic cell; **nec**, necrotic cell; **Av**, autophagic vacuoles; **apn**, apoptotic nucleus, **mn**, micronuclei. Scale bars: **A**, C, 100 nm; **B**, **D**, **E**, 500 nm.

represent the standard of care, along with targeted agents, including trastuzumab for HER2-positive tumors and ramucirumab for angiogenesis inhibition [45]. Mechanistically, these treatments either initiate apoptosis via mitochondrial pathways or inhibit proliferative signaling cascades. Nevertheless, their long-term efficacy is hindered by the occurrence of drug resistance and toxicity to healthy epithelial compartments [46]. In the search for alternative therapeutics, recent research has evidenced the promising antiproliferative and pro-apoptotic profile of α-tocopheryl succinate derivatives in gastric cancer. In this study, we evaluated the cytotoxic potential of a class of succinate derivatives – bearing various substituents on both the ester moieties and the succinate skeleton – against gastric cancer cells. These molecules were synthesized using a recently developed and innovative chemical strategy based on the alkoxy-aryloxycarbonylation of alkenes. To this end, we designed a screening approach consisting of a two-step filter methodology to identify the most effective candidates based on their cytotoxic activity. Three out of nine initially tested compounds passed the first filter (cytotoxicity step). IC_{50} values were then calculated, leading to the identification of the most potent compound, **2d**. Compound **2d** exhibited an IC_{50} value that supports its potential as a promising candidate for gastric cancer therapy. Notably, the IC_{50} of cisplatin, a standard chemotherapeutic agent widely used in gastric cancer treatment, was found to be in a similar range (approximately 20 μM) in the same cell lines. These findings indicate that the activity of compound **2d** is comparable to that of a clinically used chemotherapeutic agent, supporting its potential as an anticancer lead compound. Therefore, compound **2d** was selected for further investigation of its molecular mechanism of action. Our findings reveal that **2d** induces cell death through the modulation of both apoptosis and autophagy. In AGS cells, the apoptotic pathway is strongly activated upon exposure to **2d**, as evidenced by the marked accumulation of active Caspase-3 and cleaved PARP fragments. Concurrently – although Beclin-1 levels are slightly reduced following treatment – LC3B-II accumulates in treated cells, suggesting the activation of the autophagic process. In treated KATO III cells, Beclin-1 expression is only slightly downregulated, while LC3B lipidation is markedly augmented. Molecular markers of apoptosis are also upregulated, although to a lesser extent compared to AGS cells. The activation of either type I (apoptosis) or type II (autophagy) programmed cell death has been previously recognized as an effective antitumoral strategy shared by various chemotherapeutic agents [47]. The ability of compound **2d** to engage both pathways suggests a dual mechanism underlying its cytotoxic effects in gastric cancer cells, orchestrating the crosstalk between apoptosis and autophagy [48]. Interestingly, in AGS cells, treatment with compound **2d** reduced Beclin-1 levels while increasing LC3B-II accumulation. This molecular signature may suggest a Beclin-1-independent form of autophagy, a process previously associated with the initiation of both caspase-dependent and caspase-independent cell death pathways. Unexpectedly, Bcl-xL expression was unaffected in AGS cells and slightly increased in KATO III cells upon treatment. Given its anti-apoptotic role, this molecular profile may appear paradoxical. However, in specific cellular contexts, Bcl-2 and Bcl-xL can shift from pro-survival to pro-apoptotic inducers

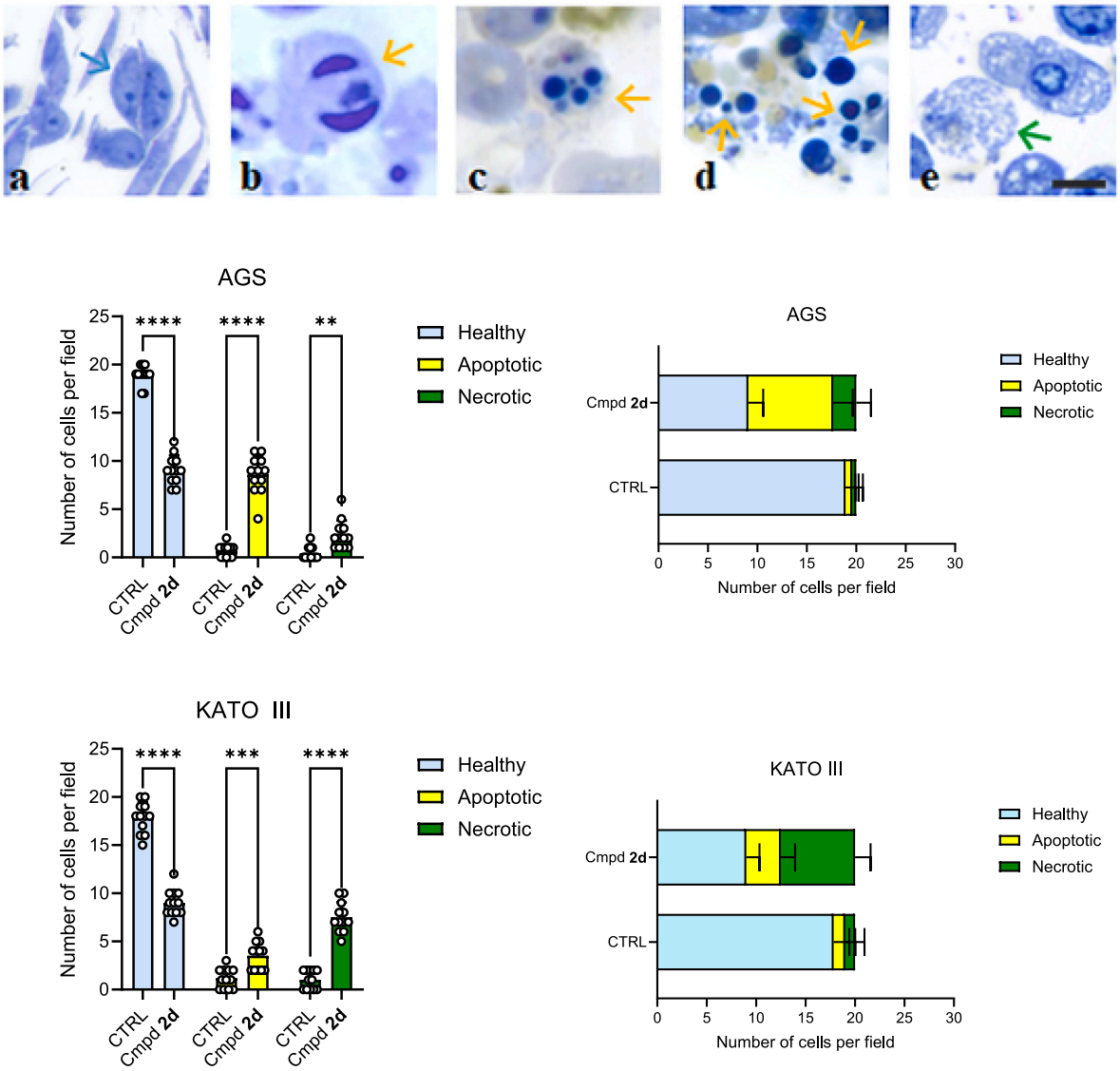

Fig. 9. The number of viable, apoptotic (early and late events), and necrotic cells under baseline conditions and following treatment with **2d** has been quantified at light microscopy. Representative images of the cells that were counted are shown in the upper part of the Figure: healthy cell (**a**); early apoptotic cell displaying crescent-shaped chromatin condensation (**b**); late apoptotic cell with micronuclei (**c**); late apoptotic cell with apoptotic bodies (**d**); necrotic cell with plasma membrane rupture (**e**). Quantification of viable, apoptotic, and necrotic cells (bottom). Data are presented as mean ± SD from twelve fields across three independent samples. Statistical significance was assessed by two-way ANOVA compared to CTRL (Šídák's multiple comparisons test), $P < 0.05$ (*), $P < 0.01$ (**), $P < 0.001$ (***), and $P < 0.0001$ (****). Scale bars: **A-H**, 1 μm; **a-d**, 50 μm.

[49,50]. As evidenced by IC_{50} values, compound **2d** is more cytotoxic in KATO III cells compared to AGS cells (19 μM vs 30.9 μM). Ultrastructural analysis revealed distinct morphological alterations in AGS and KATO III cells upon treatment. While classical apoptotic features – such as nuclear membrane detachment and chromatin condensation – were observed in both models, KATO III cells predominantly exhibited signs of necrotic cell death, characterized by plasma membrane perforation and cellular collapse. The divergent fate of AGS and KATO III cells likely results from molecular divergence downstream of shared upstream signaling pathways, involving autophagic vacuole accumulation along with mitochondrial dysfunction – as demonstrated by WB and ultrastructural analysis – ultimately leading to cell death. Overall, compound **2d** emerges as an effective cytotoxic agent in gastric cancer cells, capable of orchestrating the activation of both apoptotic and autophagic pathways. This multitarget mechanism of action enables the compound to directly promote cell death through apoptosis, while jointly potentiating autophagic activity, thereby impairing the survival capacity of cancer cells.

The therapeutic relevance of compound **2d** is further supported by the results obtained in healthy GES-1 epithelial gastric cells, which exhibited higher IC_{50} values compared to cancer cells and no activation of apoptotic or autophagic markers following treatment with 30 μM of the hit compound. Also based on preliminary computational analysis of physicochemical properties, compound **2d** appears to stand out probably due to the alkyl backbone chain that may enhance its interaction with intracellular targets. Although based on a limited dataset, the observed differences in activity between **2d** and the other derivatives suggest potential structure-activity relationships (SAR) that warrant further investigation. In conclusion, compound **2d** demonstrates significant anticancer potential by inducing apoptosis and modulating autophagy in gastric cancer cell lines. Future studies will focus on identifying and optimizing more potent derivatives to fully harness these pathways and enhance the therapeutic potential against gastric cancer. Specifically, we will focus on the modification of alkyl chain length of the succinate backbone and on the variation of the number and position

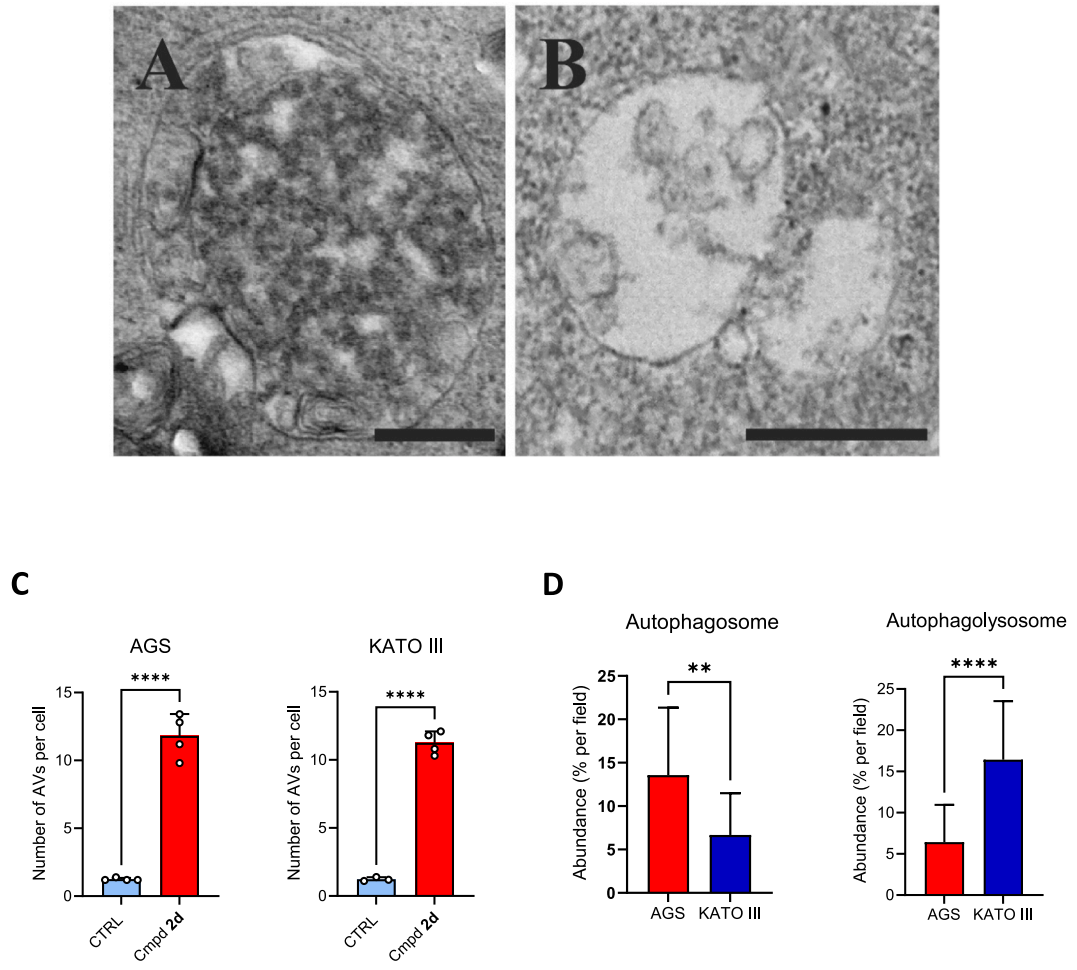

Fig. 10. TEM micrographs representative of autophagic vacuoles, including autophagosomes characterized by a double membrane enclosing cytoplasmic material (**A**) and autophagolysosomes with a single limiting membrane containing partially degraded contents (**B**). The number of autophagic vacuoles per cell (**C**) and the presence of autophagosomes and autophagolysosomes per field (**D**) are quantified for both cancer cell lines under baseline conditions and following treatment with compound **2d**. Data are expressed as mean ± SD from ten cells per condition across four different fractions. Statistical significance was assessed by unpaired *t*-test, P < 0.05 (*), P < 0.01 (**), P < 0.001 (***), and P < 0.0001 (****). Scale bars: **A**, 500 nm; **B**, 200 nm.

of hydroxyl groups on the hydroquinone moiety. Furthermore, the electronic properties of the aryl ester, introducing different EWG or EDG substituents, will be also studied. With a new set of compounds in hand, a detailed exploration of SAR to validate these preliminary trends and further optimize the molecular scaffold will be conducted, along with the determination of their ADME, toxicity, and pharmacokinetics properties. Additionally, other than testing our molecules in other cancer cell lines, we will investigate the compound's efficacy in in vivo models and evaluate potential synergistic effects when combined with standard chemotherapeutic agents or targeted therapies. By integrating these approaches, we aim to establish derivatives of compound **2d** as promising candidates to overcome resistance mechanisms and improve treatment outcomes in gastric cancer.

CRediT authorship contribution statement

Diego Olivieri: Writing – original draft, Data curation, Conceptualization. **Michele Mari:** Writing – review & editing, Data curation, Conceptualization. **Michela Battistelli:** Writing – review & editing, Visualization, Validation, Supervision, Data curation, Conceptualization. **Sabrina Burattini:** Writing – original draft, Methodology, Investigation. **Carla Carfagna:** Writing – review & editing, Data curation, Conceptualization. **Federico Gianfanti:** Writing – review & editing, Visualization, Data curation, Conceptualization. **Francesco Onesimo:** Formal analysis, Data curation. **Giovanni Bottegoni:** Data curation, Formal analysis, Software. **Riham Osman:** Methodology, Investigation, Data curation. **Nour Annous:** Investigation, Data curation. **Sara Salucci:** Writing – review & editing, Methodology, Investigation, Data curation, Conceptualization. **Ilaria Versari:** Writing – review & editing, Data curation, Conceptualization. **Irene Faenza:** Writing – review & editing, Data curation, Conceptualization. **Matteo Micucci:** Writing – original draft, Visualization, Validation, Supervision, Project administration, Data curation, Conceptualization. **Michele Retini:** Writing – review & editing, Data curation, Conceptualization.

Declaration of competing interest

The authors declare the following financial interests/personal relationships which may be considered as potential competing interests: Michela Battistelli reports that financial support was provided by University of Urbino Department of Biomolecular Sciences. Michela Battistelli reports were provided by University of Urbino Department of Biomolecular Sciences. The authors declare no conflict of interest. If there are other authors, they declare that they have no known competing financial interests or personal relationships that could have appeared to influence the work reported in this paper.

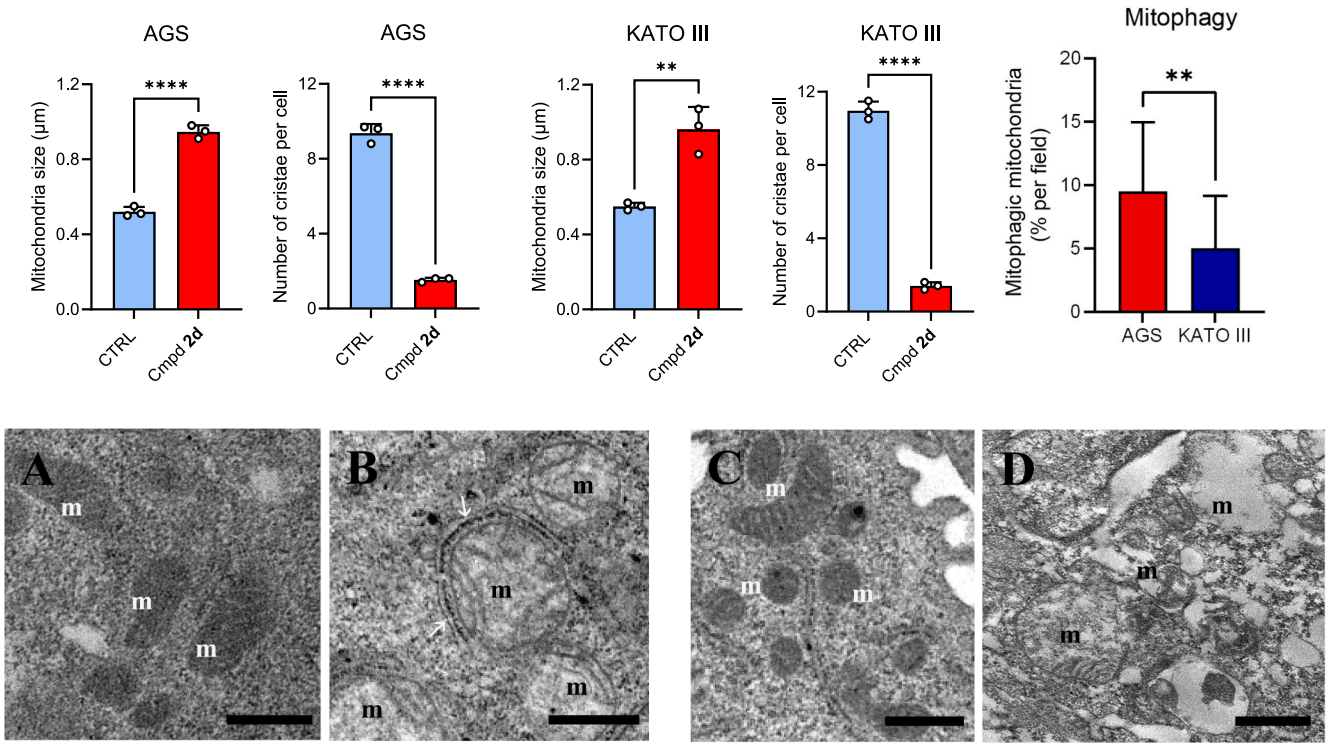

Fig. 11. Morphometric analysis of mitochondria in untreated and treated gastric cancer cells. Mitochondrial size, the number of cristae, and the proportion of damaged mitochondria surrounded by phagophores (a transient membrane structure that represents the initial stage of autophagy) were quantified and are presented in the graphs. Ultrastructural analysis (**A-D**) revealed, in AGS control cells, the presence of preserved mitochondria (**A**); these latter appeared damaged after **2d** treatment, with visible cristae reduction and surrounded by phagophore membranes (**B**). In KATO control cells, mitochondria appeared intact (**C**), whereas treated cells (**D**) showed disrupted mitochondria that were not eclosed by phagophores. Mitochondrial size is expressed as mean ± SD of four measurements across three different fractions. Cristae number is presented as mean ± SD from ten cells per condition across three different fractions. Statistical significance was assessed by unpaired t-test, $P < 0.05$ (*), $P < 0.01$ (**), $P < 0.001$ (***), and $P < 0.0001$ (****). **m**, mitochondria, →, rough endoplasmic reticulum. Scale bars: **A-D**, 1 µm.

Appendix A. Supplementary data

Supplementary data to this article can be found online at https://doi.org/10.1016/j.bioorg.2026.109997.

Data availability

Data will be made available on request.

References

[1] A.E. Dassen, J.L. Dikken, K. Bosscha, M.W.J.M. Wouters, A. Cats, C.J.H. van de Velde, J.-W. Coebergh, V.E.P.P. Lemmens, Gastric cancer: decreasing incidence but stable survival in the Netherlands, Acta Oncol. (Madr) 53 (2014) 138–142, https://doi.org/10.3109/0284186X.2013.789139.

[2] R.E. Sexton, M.N. Al Hallak, M. Diab, A.S. Azmi, Gastric cancer: a comprehensive review of current and future treatment strategies, Cancer Metastasis Rev. 39 (2020) 1179–1203, https://doi.org/10.1007/s10555-020-09925-3.

[3] T.I. Mamun, S. Younus, Md.H. Rahman, Gastric cancer—epidemiology, modifiable and non-modifiable risk factors, challenges and opportunities: an updated review, Cancer Treat. Res. Commun. 41 (2024) 100845, https://doi.org/10.1016/j.ctarc.2024.100845.

[4] M. Micucci, B.-Z. Xiang, C.-M. Ting, H.-Y. Kwan, M. Mari, M. Retini, S. Burattini, R. Osman, U.J. Okeke, F.O. Abdullah, F. Gianfanti, M. Battistelli, Matching traditional Chinese medicine and Western medicine-based research: advanced nutraceutical development for proactive gastric cancer prevention, World J. Gastrointest. Oncol. 16 (2024) 3798–3819, https://doi.org/10.4251/wjgo.v16.i9.3798.

[5] M. Micucci, M. Battistelli, S. Burattini, M. Mari, M. Retini, R. Osman, I. Versari, A. B. Stella, F. Gianfanti, J.O. Udodinma, F. Onesimo, S. Riela, M. Canale, A. P. Piccionello, I. Faenza, S. Salucci, Food waste to wellness: a grape pomace blend in gastric Cancer prevention, Food Sci. Nutr. 13 (2025), https://doi.org/10.1002/fsn3.70350.

[6] L.E. Wroblewski, R.M. Peek Jr., Clinical pathogenesis, in: Molecular Mechanisms of Gastric Cancer Development, 2023, pp. 25–52, https://doi.org/10.1007/978-3-031-47331-9_2.

[7] A.R. Siebenhüner, S. De Dosso, D. Helbling, C. Astaras, P. Szturz, P. Moosmann, S. Pederiva, T. Winder, P. Von Burg, M. Borner, Advanced gastric Cancer: current treatment landscape and a future outlook for sequential and personalized guide: Swiss expert statement article, Oncol. Res. Treat. 44 (2021) 485–494, https://doi.org/10.1159/000518107.

[8] S.S. Joshi, B.D. Badgwell, Current treatment and recent progress in gastric cancer, CA Cancer J. Clin. 71 (2021) 264–279, https://doi.org/10.3322/caac.21657.

[9] C.S. Fuchs, D. Niedzwiecki, H.J. Mamon, J.E. Tepper, X. Ye, R.S. Swanson, P. C. Enzinger, D.G. Haller, T. Dragovich, S.R. Alberts, G.A. Bjarnason, C.G. Willett, L. L. Gunderson, R.M. Goldberg, A.P. Venook, D. Ilson, E. O'Reilly, K. Ciombor, D. J. Berg, J. Meyerhardt, R.J. Mayer, Adjuvant chemoradiotherapy with Epirubicin, cisplatin, and fluorouracil compared with adjuvant chemoradiotherapy with fluorouracil and leucovorin after curative resection of gastric Cancer: results from CALGB 80101 (Alliance), J. Clin. Oncol. 35 (2017) 3671–3677, https://doi.org/10.1200/JCO.2017.74.2130.

[10] M.H. Kulke, B. Wu, J.W. Clark, P.C. Enzinger, T.J. Lynch, M. Vincitore, A. Michelini, C.S. Fuchs, A phase II study of doxorubicin, cisplatin, and 5-fluorouracil in patients with advanced adenocarcinoma of the stomach or Esophagus, Cancer Investig. 24 (2006) 229–234, https://doi.org/10.1080/07357900600633924.

[11] H.-M. Hu, H.-J. Tsai, H.-Y. Ku, S.-S. Lo, Y.-S. Shan, H.-C. Chang, Y. Chao, J.-S. Chen, S.-C. Chen, C.-J. Chiang, A.F.-Y. Li, H.-P. Wang, T.-E. Wang, L.-Y. Bai, M.-S. Wu, L.-T. Chen, T.-W. Liu, Y.-H. Yang, Survival outcomes of management in metastatic gastric adenocarcinoma patients, Sci. Rep. 11 (2021) 23142, https://doi.org/10.1038/s41598-021-02391-z.

[12] A. Kazemi, M. Goodarzi, K. Daneshipour, H. Sarabadani, Z. Shahpar, B.S. Hajiagha, H. Kheradjoo, S. Mohammadzadehsaliani, Unrevealing the vital role of ncRNAs in gastric Cancer chemoresistance, Pathol. Res. Pract. 250 (2023) 154761, https://doi.org/10.1016/j.prp.2023.154761.

[13] K. Shitara, Y.-J. Bang, S. Iwasa, N. Sugimoto, M.-H. Ryu, D. Sakai, H.-C. Chung, H. Kawakami, H. Yabusaki, J. Lee, K. Saito, Y. Kawaguchi, T. Kamio, A. Kojima, M. Sugihara, K. Yamaguchi, Trastuzumab Deruxtecan in previously treated HER2-positive gastric Cancer, N. Engl. J. Med. 382 (2020) 2419–2430, https://doi.org/10.1056/NEJMoa2004413.

[15] A. Topcu, M.M. Atci, S. Secmeler, M. Besiroglu, M. Ayhan, M. Ozkan, O. Bozkurt, Z. Urakci, S. Ay, C. Geredeli, A.I. Yasin, H.M. Turk, Efficacy of trastuzumab and potential risk factors on survival in patients with HER2-positive metastatic gastric Cancer, Future Oncol. 17 (2021) 4157–4169, https://doi.org/10.2217/fon-2021-0398.

[16] C.S. Fuchs, J. Tomasek, C.J. Yong, F. Dumitru, R. Passalacqua, C. Goswami, H. Safran, L.V. dos Santos, G. Aprile, D.R. Ferry, B. Melichar, M. Tehfe, E. Topuzov, J.R. Zalcberg, I. Chau, W. Campbell, C. Sivanandan, J. Pikiel, M. Koshiji, Y. Hsu, A. M. Liepa, L. Gao, J.D. Schwartz, J. Tabernero, Ramucirumab monotherapy for previously treated advanced gastric or gastro-oesophageal junction adenocarcinoma (REGARD): an international, randomised, multicentre, placebo-controlled, phase 3 trial, Lancet 383 (2014) 31–39, https://doi.org/10.1016/S0140-6736(13)61719-5.

[17] M. Garrido, The safety and efficacy of ramucirumab in combination with paclitaxel for the treatment of advanced gastric or gastro-esophageal junction adenocarcinoma, Expert. Rev. Anticancer. Ther. 16 (2016) 1005–1010, https://doi.org/10.1080/14737140.2016.1231576.

[18] E. Varone, M. Retini, A. Cherubini, A. Chernorudskiy, A. Marrazza, A. Guidarelli, A. Cagnotto, M. Beeg, M. Gobbi, S. Fumagalli, M. Bolis, L. Guarrera, M.C. Barbera, C. Grasselli, A. Bleve, D. Generali, M. Milani, M. Mari, M. Salmona, G. Piersanti, G. Bottegoni, M. Broggini, Y.M.W. Janssen-Heininger, J. Cho, O. Cantoni, E. Zito, Small molecule-mediated inhibition of the oxidoreductase ERO1A restrains aggressive breast cancer by impairing VEGF and PD-L1 in the tumor microenvironment, Cell Death Dis. 16 (2025) 105, https://doi.org/10.1038/s41419-025-07426-1.

[19] Y. Zhao, X. Zhao, B. Yang, J. Neuzil, K. Wu, A-Tocopheryl succinate-induced apoptosis in human gastric cancer cells is modulated by ERK1/2 and c-Jun N-terminal kinase in a biphasic manner, Cancer Lett. 247 (2007) 345–352, https://doi.org/10.1016/j.canlet.2006.05.015.

[20] X. Huang, Z. Zhang, L. Jia, Y. Zhao, X. Zhang, K. Wu, Endoplasmic reticulum stress contributes to vitamin E succinate-induced apoptosis in human gastric cancer SGC-7901 cells, Cancer Lett. 296 (2010) 123–131, https://doi.org/10.1016/j.canlet.2010.04.002.

[21] F. Bartoccini, F. Fanini, M. Retini, G. Piersanti, General synthesis of unnatural 4-, 5-, 6-, and 7-bromo-d-tryptophans by means of a regioselective indole alkylation, Tetrahedron Lett. 61 (2020) 151923, https://doi.org/10.1016/j.tetlet.2020.151923.

[22] H. Wu, S. Liu, J. Gong, J. Liu, Q. Zhang, X. Leng, N. Zhang, Y. Li, VCPA, a novel synthetic derivative of α-tocopheryl succinate, sensitizes human gastric cancer to doxorubicin-induced apoptosis via ROS-dependent mitochondrial dysfunction, Cancer Lett. 393 (2017) 22–32, https://doi.org/10.1016/j.canlet.2017.02.007.

[23] K. Wu, Y. Zhao, G.-C. Li, W.-P. Yu, C-Jun N-terminal kinase is required for vitamin E succinate-induced apoptosis in human gastric cancer cells, World J. Gastroenterol. 10 (2004) 1110, https://doi.org/10.3748/wjg.v10.i8.1110.

[24] Y. Sun, Y. Zhao, L. Hou, X. Zhang, Z. Zhang, K. Wu, RRR-α-tocopheryl succinate induces apoptosis in human gastric cancer cells via the NF-κB signaling pathway, Oncol. Rep. 32 (2014) 1243–1248, https://doi.org/10.3892/or.2014.3282.

[25] D. Olivieri, R. Tarroni, N. Della Ca', R. Mancuso, B. Gabriele, G. Spadoni, C. Carfagna, Bis-alkoxycarbonylation of acrylic esters and amides for the synthesis of 2-alkoxycarbonyl or 2-carbamoyl succinates, Adv. Synth. Catal. 362 (2020) 533–544, https://doi.org/10.1002/adsc.201900918.

[26] D. Olivieri, R. Tarroni, N. Della Ca', R. Mancuso, B. Gabriele, G. Spadoni, C. Carfagna, Combined effect of palladium catalyst and the alcohol to promote the uncommon bis-Alkoxycarbonylation of allylic substrates, ChemCatChem 14 (2022), https://doi.org/10.1002/cctc.202101923.

[27] D. Olivieri, R. Tarroni, S. Zacchini, N. Della Ca', R. Mancuso, B. Gabriele, G. Spadoni, C. Carfagna, Regioselective one-step alkoxy-aryloxycarbonylation of alkenes, J. Catal. 421 (2023) 431–440, https://doi.org/10.1016/j.jcat.2023.03.008.

[28] D. Olivieri, M. Verboni, R. Tarroni, S. Zacchini, S. Lucarini, N. Della Ca', R. Mancuso, B. Gabriele, C. Carfagna, Versatile stereoselective oxidative alkoxycarbonylation of styrenes at room-temperature, J. Catal. 432 (2024) 115397, https://doi.org/10.1016/j.jcat.2024.115397.

[29] D. Olivieri, F. Fini, R. Mazzoni, S. Zacchini, N. Della Ca', G. Spadoni, B. Gabriele, R. Mancuso, V. Zanotti, C. Carfagna, Diastereospecific bis-alkoxycarbonylation of 1,2-disubstituted olefins catalyzed by aryl α-diimine palladium(II) catalysts, Adv. Synth. Catal. 360 (2018) 3507–3517, https://doi.org/10.1002/adsc.201701597.

[30] F. Fini, M. Beltrani, R. Mancuso, B. Gabriele, C. Carfagna, Selective aryl α-Diimine/palladium-catalyzed bis-alkoxy- carbonylation of olefins for the synthesis of substituted succinic diesters, Adv. Synth. Catal. 357 (2015) 177–184, https://doi.org/10.1002/adsc.201400501.

[31] S.E. Byeon, Y.-S. Yi, J. Lee, W.S. Yang, J.H. Kim, J. Kim, S. Hong, J.-H. Kim, J. Y. Cho, Hydroquinone exhibits in vitro and in vivo anti-Cancer activity in Cancer cells and mice, Int. J. Mol. Sci. 19 (2018) 903, https://doi.org/10.3390/ijms19030903.

[32] R.M. Giner, J.L. Rios, S. Máñez, Antioxidant activity of natural Hydroquinones, Antioxidants 11 (2022) 343, https://doi.org/10.3390/antiox11020343.

[33] D. Xie, K. Han, Q. Jiang, S. Xie, J. Zhou, Y. Zhang, J. Xu, Y. He, P. Zhao, X. Yang, Design, synthesis, and inhibitory activity of hydroquinone ester derivatives against mushroom tyrosinase, RSC Adv. 14 (2024) 6085–6095, https://doi.org/10.1039/d4ra00007b.

[34] R. Ballini, G. Bosica, D. Fiorini, P. Righi, Nitroalkanes and dimethyl maleate as source of 3-alkyl succinic anhydrides and (*E*)-3-alkylidene succinic anhydrides, Synthesis 5 (2002) 0681–0685, https://doi.org/10.1055/s-2002-23548.

[35] P. Linciano, G. Cullia, C. Borsari, M. Santucci, S. Ferrari, G. Witt, S. Gul, M. Kuzikov, B. Ellinger, N. Santarém, A. Cordeiro da Silva, P. Conti, M. L. Bolognesi, M. Roberti, F. Prati, F. Bartoccini, M. Retini, G. Piersanti, A. Cavalli, L. Goldoni, S.M. Bertozzi, F. Bertozzi, E. Brambilla, V. Rizzo, D. Piomelli, A. Pinto, T. Bandiera, M.P. Costi, Identification of a 2,4-diaminopyrimidine scaffold targeting Trypanosoma brucei pteridine reductase 1 from the LIBRA compound library screening campaign, Eur. J. Med. Chem. 189 (2020) 112047, https://doi.org/10.1016/j.ejmech.2020.112047.

[36] S.D. Ittel, L.K. Johnson, M. Brookhart, Late-metal catalysts for ethylene Homo- and copolymerization, Chem. Rev. 100 (2000) 1169–1204, https://doi.org/10.1021/cr9804644.

[37] C. Carfagna, G. Gatti, P. Paoli, B. Binotti, F. Fini, A. Passeri, P. Rossi, B. Gabriele, New aryl α-Diimine palladium(II) catalysts in Stereocontrolled CO/vinyl Arene copolymerization, Organometallics 33 (2014) 129–144, https://doi.org/10.1021/om400887x.

[38] A. Schuffenhauer, N. Schneider, S. Hintermann, D. Auld, J. Blank, S. Cotesta, C. Engeloch, N. Fechner, C. Gaul, J. Giovannoni, J. Jansen, J. Joslin, P. Krastel, E. Lounkine, J. Manchester, L.G. Monovich, A.P. Pelliccioli, M. Schwarze, M. D. Shultz, N. Stiefl, D.K. Baeschlin, Evolution of Novartis' small molecule screening deck design, J. Med. Chem. 63 (23) (2020) 14425–14447, https://doi.org/10.1021/acs.jmedchem.0c01332. Epub 2020 Nov 3. PMID: 33140646.

[39] M. Micucci, A. Stella Bartoletti, F.O. Abdullah, S. Burattini, I. Versari, M. Canale, F. D'Agostino, D. Roncarati, D. Piatti, G. Sagratini, G. Caprioli, M. Mari, M. Retini, I. Faenza, M. Battistelli, S. Salucci, Paradigm shift in gastric Cancer prevention: harnessing the potential of Aristolochia olivieri extract, Int. J. Mol. Sci. 24 (2023) 16003, https://doi.org/10.3390/ijms242116003.

[40] S.M. Khirallah, H.M.M. Ramadan, H.A.A. Aladl, N.O. Ayaz, L.A.F. Kurdi, M. Jaremko, S.Z. Alshawwa, E.M. Saied, Antidiabetic potential of novel 1,3,5-Trisubstituted-2-Thioxoimidazloidin-4-one analogues: insights into α-glucosidase, α-amylase, and antioxidant activities, Pharmaceuticals (Basel) 15 (2022) 1576, https://doi.org/10.3390/ph15121576.

[41] A.R. Alzahrani, D.I. Mohamed, H.H. Abo Nahas, D. Alaa El-Din Aly El-Waseef, A. S. Altamimi, I.H. Youssef, I.A.A. Ibrahim, S.M.Y. Mohamed, Y.G. Sabry, A. H. Falemban, N.A. Elhawary, G.A. Bamagous, M. Jaremko, E.M. Saied, Trimetazidine alleviates bleomycin-induced pulmonary fibrosis by targeting the long noncoding RNA CBR3-AS1-mediated miRNA-29 and Resistin-like molecule alpha 1: deciphering a novel trifecta role of LncRNA CBR3-AS1/miRNA-29/FIZZ1 axis in lung fibrosis, Drug Des. Devel. Ther. 18 (2024) 3959–3986, https://doi.org/10.2147/DDDT.S463626.

[42] M.M. Labib, A.M. Alqahtani, H.H. Abo Nahas, R.M. Aldossari, B.F. Almiman, S. Ayman Alnumaani, M. El-Nablaway, E. Al-Olayan, M. Alsunbul, E.M. Saied, Novel insights into the antimicrobial and antibiofilm activity of pyrroloquinoline quinone (PQQ); *in vitro*, *in silico*, and shotgun proteomic studies, Biomolecules 14 (2024) 1018, https://doi.org/10.3390/biom14081018.

[43] Z. He, Y. Zhou, J. Liu, N. Li, H. Fan, The intersection of helicobacter pylori and gastric cancer: signaling pathways and molecular mechanisms, Front. Cell. Infect. Microbiol. 15 (2025), https://doi.org/10.3389/fcimb.2025.1601501.

[44] Y. Liang, K. Liu, V. Kudriashov, L. Sun, W. Zhang, X. Chen, L. Zhao, X. Song, K. Yang, J. Hu, Comparison among early-onset, late-onset, and conventional-onset adenocarcinoma of stomach and esophagogastric junction: a retrospective study, World J. Surg. Oncol. 23 (2025) 222, https://doi.org/10.1186/s12957-025-03867-2.

[45] S. Wu, P. Xu, F. Zhang, Advances in targeted therapy for gastric cancer based on tumor driver genes, J. Zhejiang Univ. (Med. Sci.) 53 (2024) 73–83, https://doi.org/10.3724/zdxbyxb-2023-0522.

[46] M. Sorokin, E. Poddubskaya, M. Baranova, A. Glusker, L. Kogoniya, E. Markarova, D. Allina, M. Suntsova, V. Tkachev, A. Garazha, M. Sekacheva, A. Buzdin, RNA sequencing profiles and diagnostic signatures linked with response to ramucirumab in gastric cancer, Molecular Case Studies 6 (2020) a004945, https://doi.org/10.1101/mcs.a004945.

[47] W. Nie, L. Hu, Z. Yan, Q. Wang, S. He, X. Gao, F. Yang, Study on the regulation of gastric cancer cell apoptosis by LACTB through mitochondrial autophagy pathway, Sci. Rep. 15 (2025) 23273, https://doi.org/10.1038/s41598-025-06047-0.

[48] R. Kang, H.J. Zeh, M.T. Lotze, D. Tang, The Beclin 1 network regulates autophagy and apoptosis, Cell Death Differ. 18 (2011) 571–580, https://doi.org/10.1038/cdd.2010.191.

[49] F. Zhou, Y. Yang, D. Xing, Bcl-2 and Bcl-xL play important roles in the crosstalk between autophagy and apoptosis, FEBS J. 278 (2011) 403–413, https://doi.org/10.1111/j.1742-4658.2010.07965.x.

[50] J. Hagenbuchner, M.J. Ausserlechner, V. Porto, R. David, B. Meister, M. Bodner, A. Villunger, K. Geiger, P. Obexer, The anti-apoptotic protein BCL2L1/BCL-xL is neutralized by pro-apoptotic PMAIP1/Noxa in neuroblastoma, thereby determining bortezomib sensitivity independent of Prosurvival MCL1 expression, J. Biol. Chem. 285 (2010) 6904–6912, https://doi.org/10.1074/jbc.M109.038331.

Update

Bioorganic Chemistry
Volume 179, Issue , 5 September 2026, Page

DOI: https://doi.org/10.1016/j.bioorg.2026.110024

Bioorganic Chemistry 179 (2026) 110024

Contents lists available at ScienceDirect

Bioorganic Chemistry

journal homepage: www.elsevier.com/locate/bioorg

Corrigendum

Corrigendum to "Synthesis and biological evaluation of mixed aryl-alkyl succinates as modulators of autophagy and apoptosis in gastric carcinoma" [Bioorg. Chem. 179 (2026) 109997]

Diego Olivieri [a,1], Michele Mari [a,1], Michela Battistelli [a,*], Sabrina Burattini [a], Carla Carfagna [b], Federico Gianfanti [a,*], Francesco Onesimo [a], Giovanni Bottegoni [a], Riham Osman [a], Nour Annous [a], Sara Salucci [c], Ilaria Versari [c], Irene Faenza [c], Matteo Micucci [a], Michele Retini [a]

[a] Department of Biomolecular Sciences, University of Urbino Carlo Bo, 61029 Urbino, Italy
[b] Department of Industrial Chemistry "Toso Montanari", University of Bologna, Via Piero Gobetti 85, 40129 Bologna, BO, Italy
[c] Department of Biomedical and NeuroMotor Sciences, University of Bologna, 40126 Bologna, Italy

The authors regret.

Diego Olivieri [a1], Michele Mari [a1], Michela Battistelli [a], Sabrina Burattini [a], Carla Carfagna [b], Federico Gianfanti [a], Francesco Onesimo [a], Giovanni Bottegoni [a], Riham Osman [a], Nour Annous [a], Sara Salucci [c], Ilaria Versari [c], Irene Faenza [c], Matteo Micucci [a], Michele Retini [a]

Diego Olivieri and Michele Mari contributed equally to this work ([1]).

Matteo Micucci and Michele Retini dont't contribute equally to this work, so Micucci was uncorrectly designated as co–last.

The authors would like to apologise for any inconvenience caused.

DOI of original article: https://doi.org/10.1016/j.bioorg.2026.109997.

* Corresponding authors.
E-mail addresses: michela.battistelli@uniurb.it (M. Battistelli), federico.gianfanti@uniurb.it (F. Gianfanti).

[1] These authors contributed equally to this work.

https://doi.org/10.1016/j.bioorg.2026.110024

Available online 29 May 2026